the
abdus salam
international centre for theoretical physics

SMR: 1098/9

WORKSHOP ON THE STRUCTURE OF BIOLOGICAL MACROMOLECULES

(16 - 27 March 1998)

"Synchrotron Radiation in Structural Biology"

An Introduction to Mad (Multiwavelength Anomalous Diffraction)

presented by:

Adolfo SAVOIA

Sincrotrone Trieste S.c.p.A.
S.S. 14 Km 163,5
34012 Basovizza - Trieste
Italy

AN INTRODUCTION TO MAD

(MULTIWAVELENGTH ANOMALOUS DIFFRACTION)

Franco ZANINI and Adolfo SAVOIA

SINCROTRONE TRIESTE S.c.p.A.
S.S. 14 Km 163,5
34012 Basovizza-Trieste

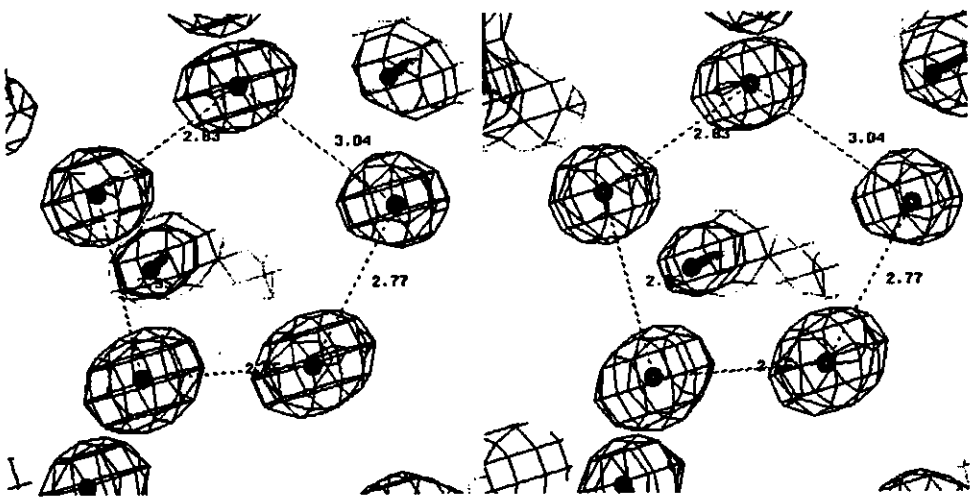

1. X-Ray Diffraction and the Phase Problem

X-ray diffraction is related to the elastic emission of radiation due to acceleration of electrons in response to an incident electromagnetic wave. When an incident wave stimulates multiple scattering centers, the scattered waves add together and interfere with one another, and thus the total scattering from an object is sensitive to internal structure. If we know the electron-density distribution of a scattering object of volume V we can write the total scattered wave $F(\vec{S})$ normalized to the scattering from a free electron in the wavevector direction $\hat{k}$

$$F(\vec{S}) = \iiint \rho(\vec{r}) \exp(2\pi i \vec{S} \cdot \vec{r}) dV \tag{1}$$

where

$$\vec{S} = (\hat{k} - \hat{k}_0)/\lambda \tag{2}$$

for incident x-rays of given wavelength λ directed along $\hat{k}_0$ (Drenth, 1994). In a real experiment, we would like to calculate the inverse, i.e. to obtain the structure of the sample given the scattering. Fortunately, it can be easily shown that the electron density can be calculated by a simple Fourier anti-transform, even if this solution leaves another open question. Since we can only measure the intensity (i.e. a square modulus) of scattering, we are not able to derive directly the scattering phase.

It is evident that the evaluation of atomic parameters from the direct analysis of X-ray diffraction patterns is rather complicated. Thanks to direct-method analyses, using statistical relations among the diffracted intensities, small-molecule structures are now solved routinely. Unfortunately, except in few cases, the same methods cannot be applied to macromolecules.

A set of initial phases for a macromolecule structure can be extracted using the method of isomorphous replacement with heavy atoms (Green *et al.*, 1954, Blundell and Johnson, 1976). If heavy atoms bind specifically to the molecule, their position can be identified, and the phase problem can be solved from the differences in the structure factors between native and derivative crystals, known as isomorphous differences. The calculated contribution from this known centers can be used as reference waves for deducing the correct phases of the native crystal structure from the observed modulations caused by their presence. In general, because of possible ambiguities, multiple isomorphous replacement

(MIR) is often used, as well as other computational procedures such as solvent flattening or molecular averaging.

Solvent flattening is a noise filtering technique which makes use of the fact that in protein crystals there are large regions of disordered solvent where the map should be almost empty. The map is modified by depressing weak features below a threshold which is calculated from the estimated solvent content. Phases are then calculated with a convergence method from the modified map. Molecular averaging is often used in conjunction with solvent flattening, and can lead to substantial improvements of the map. The first step is to determine the symmetry transformations for averaging (from heavy atom positions or molecular replacement), then a molecular envelope is determined with programs like Demon or RAVE.

Obtaining suitable heavy atom derivatives is the main difficulty of the isomorphous replacement technique. As a result of recombinant DNA technology, for example, cysteines can now be inserted into proteins to produce mercury derivatives. However, the engineering of cysteins does not guarantee mercurial derivatives or even the isomorphism of derivative crystals.

Over the last few years, the crystallographic technique known as MAD, or multiwavelength anomalous diffraction, has emerged as one of the more powerful methodologies available to the macromolecular crystallographer (Yang *et al.,* 1990, Tesmer *et al.,* 1994, Glover *et al.,* 1995, Todd *et al.*). MAD is based on the use of anomalous scattering measurements at appropriate energies, taking into account the strong variations of the scattering factor near an absorption edge.

Although MAD and MIR look different, the physics underlying these two techniques is the same. In both methods, the scattering at a few specific locations in the unit cell is changed. In MIR, this is done by the introduction of heavy atoms at specific locations, whereas in MAD the scattering of pre-existing atoms is varied by changing the x-ray wavelength. Before the availability of synchrotrons to serve as tunable x-ray sources, conventional MIR using heavy atom derivatives was the only practical solution. Thus MAD can be considered an ideal case of MIR: because the changes in scattering used by MAD derive from physical changes to crystals rather than chemical changes, lack of isomorphism among multiple data sets cannot occur, and the structure determinations have the potential to be rapid and direct.

2. *Anomalous scattering*

The classical derivation of the physical basis for anomalous scattering is developed by treating the scattering interaction as a pair of coupled oscillators. One oscillator is the incident x-ray wave; the other is the scattering atom treated as a dipole oscillator with frequency equal to the observed value of an absorption edge. This theory is treated in a not intuitive way by James (1948), and we will give here only a basic description in terms of the scattering cross section of an atom as seen by an incident x-ray photon (Hendrickson, 1991). The structural dependence of the intensity $I(\vec{h})$ for a reflection identified by indices $\vec{h}(h,k,l)$ is given by

$$I(\vec{h}) \propto | F(\vec{h}) |^2 \tag{3}$$

where

$$F(\vec{h}) = \sum_{j}^{atom} f_j \exp(-B_j s)\exp(2\pi\vec{h}\cdot\vec{x}_j) \tag{4}$$

is the structure factor, f_j is the atomic scattering factor for the j-th atom of the crystal, $s = \sin\vartheta/\lambda$ (where ϑ is the Bragg angle of reflection), B_j is the j=th atomic thermal parameter and $\vec{x}_j(x,y,z)$ defines the j-th atomic position vector. When the incident photon has relatively low energy:

- The photon is either scattered or not, but is not absorbed as it has insufficient energy to excite any of the available electronic transitions.
- The scattering cross-section of the atom may be adequately described by using the normal atomic scattering coefficient f_0.
- The photon is scattered with no phase delay.

The atomic scattering factor is related to the coherent scattering from a single atom for the Thompson scattering of a free electron. This factor includes a component that depends only on the electron density distribution in the atom, but can also include a wavelength-dependent component related to bound electronic states in the atom.

When the incident photon has high enough energy:

- Some photons are scattered normally.
- Some photons are absorbed and re-emitted at lower energy (fluorescence).
- Some photons are absorbed and immediately re-emitted at the same energy (strong coupling to absorption edge energy).

- The scattered photon gains an imaginary component to its phase; i.e. it is phase-retarded compared to a normally scattered photon.

This effect is most easily measured as a function of x-ray energy by noting either the sharp increase in absorption or in fluorescence (fig.1). The anomalous dispersion of x-ray optical properties is caused by the resonant absorption of energy in the transition from a bound atomic orbital to an electronic state in the continuum. The atomic scattering factor f_0 for normal scattering is purely real, independent of wavelength, and falls off with scattering angles. The anomalous scattering component f_Δ, in contrast, is complex, is strongly wavelength-dependent, and is virtually independent of scattering angle. The total scattering factor is then:

$$f = f_0 + | f_\Delta | e^{i\delta} = f_0 + f' + if'' \tag{5}$$

where f' and f'' are the real and imaginary components of the anomalous scattering. The scattering components f' and f'' are related by the Kramers-Kronig relationships.

$$f'(\omega) = \frac{2}{\pi}\int_0^\infty \frac{\omega^2 f''(\omega')\partial\omega'}{\omega^2 - \omega'^2} \tag{6a}$$

$$f''(\omega) = -\frac{2\omega}{\pi}\int_0^\infty \frac{[f'(\omega') - 1]\partial\omega'}{\omega^2 - \omega'^2} \tag{6b}$$

Once the f'' spectrum is obtained experimentally from the sample crystal via fluorescence measurements, the corresponding f' spectrum may be calculated by numerical integration using the above equation. In figure 1 we can see experimental values of f' and f'' derived from an x-ray absorption spectrum of selenomethionyl thioredoxin from E. Coli.

The Cromer/Liberman theoretical values for scattering factors are not accurate for energies very near an absorption edge. Here the interaction of the scattering atom with its chemical neighbours complicates the scattering behaviour considerably. Shown in figure 2 is a comparison of the theoretical values of f'' with the values determined experimentally for the selenium site of selenomethionyl thioredoxin. The f' values can be derived from the corresponding f'' spectra via the Kramers-Kronig equation.

Note in particular:

- The actual absorption edge is shifted relative to the idealised edge for an isolated Eu atom. The largest part of this shift is due to the oxidation state of the Eu atom in the protein.

- The local chemical environment introduces "ripples" (EXAFS) into the scattering spectrum.
- The maximum achievable f'' is actually larger than the edge jump from theory. (The effect isn't very large in this particular example, but sometimes it is substantial).
- The maximum achievable $|f'|$, however, is smaller than the theoretical value. This is largely limited by the energy bandwidth of the x-ray source.

The anomalous scattering profiles for isolated atoms of few selected elements is shown in fig. 3. These examples illustrate a number of additional considerations:

- Edge positions for a given orbital occur at systematically increasing energies (or shorter wavelengths) as the atomic number increases.
- Apart from the energy of transition, all K edges are essentially alike and all L edges are alike.
- L_{III} edges, which are associated with two of the six *2p* electrons, have anomalous scattering magnitudes on the order of three times greater than those for K edges, which are associated with the two *1s* electrons.

The anomalous scattering profile s which are usually observed from molecules, however, are typically more featured than the calculated ones for isolated atoms. These resonant "white line" features, which are related to transitions to unoccupied molecular orbitals, can be threefold greater than those expected from isolated atoms (Templeton *et al.*, 1982).

3. Multiwavelength Anomalous Diffraction (MAD)

Figure 4 shows data for the variation of f' and f'', the real and imaginary components of the anomalous scattering of selenium, around its K-edge at 0.98 Å. Variation of the wavelength around the K-edge, where f' and f'' for selenium change significantly, results in a change in the scattering from the selenium atoms, leading to intensity differences between wavelengths as well as between Friedel pairs (i.e. reflections h,k,l and -h,-k,-l) within a wavelength. The basic idea is that if we can locate the anomalous scattering atoms within the unit cell (those contributing to the anomalous scattering contribution from all atoms) then we can calculate the corresponding phase angle. The MAD phasing equations of Karle (1980) can then be used to generate an estimate for $|F_{0T}|$, the normal scattering component of all atoms and the difference in phase angle between normal and anomalous scattering components. A Fourier transform of $|F_{0T}|$ and their phases φ_{0A} should yield an electron density map corresponding to all atoms in the structure.

During the last years, several structures have been solved using the formalism developed by Hendrickson (1985) on the basis of Karle equations: in his approach the impact of anomalous scattering on diffraction data can be evaluated by substituting the scattering factor expression (5) into the structure factor equation (4) and writing the squared modulus which is directly related to the actual diffraction measurement (3). In the case of a single kind of anomalous scatterer, it is easy to separate known wavelength-dependent factors form unknown wavelength-independent variables. The total structure factor obtained at a particular wavelength λ for a particular reflection $\vec{h}$ is denoted $F_\lambda(\vec{h})$. The wavelength-invariant contribution from the normal f_0 components of the scattering factors is given by $F_{0T} = \mid F_{0T} \mid \exp i\varphi_{0T}$, while the part contributed only by the normal scattering component of the anomalous center is given by $F_{0A} = \mid F_{0A} \mid \exp i\varphi_{0A}$. Then

$$\begin{aligned} \mid F_\lambda(\pm\vec{h}) \mid^2 \quad = \mid F_{0T} \mid^2 \qquad & +a(\lambda) \mid F_{0A} \mid^2 \\ & +b(\lambda) \mid F_{0T} \mid\mid F_{0A} \mid \cos(\varphi_{0T} - \varphi_{0A}) \\ & \pm c(\lambda) \mid F_{0T} \mid\mid F_{0A} \mid \sin(\varphi_{0T} - \varphi_{0A}) \end{aligned} \tag{7}$$

where

$$a(\lambda) = (f'^2 + f''^2)/f_0^2 \tag{8a}$$
$$b(\lambda) = 2(f'/f_0) \tag{8b}$$
$$c(\lambda) = 2(f''/f_0) \tag{8c}$$

The difference between the structure amplitudes of Friedel pairs, or rotational symmetry equivalents of them

$$\Delta F_{\pm h} = \mid F_\lambda(\vec{h}) \mid - \mid F_\lambda(-\vec{h}) \mid \tag{9}$$

is the so-called Bijvoet difference. In absence of anomalous scattering this difference is zero. From eq. 7 we can see that it depends on $f''(\lambda)$ and $\sin(\varphi_{0T} - \varphi_{0A}) = \sin\Delta\varphi$. The difference

$$\Delta F_{\Delta\lambda} = \overline{\mid F_{\lambda_i} \mid} - \overline{\mid F_{\lambda_j} \mid} \tag{10}$$

where $\overline{\mid F_\lambda \mid} = (\mid F_\lambda(\vec{h}) + F_\lambda(-\vec{h}) \mid)/2$ is the so-called dispersive difference. This, in turn, depends on $\cos(\Delta\varphi)$ and on $\mid f'(\lambda_i) - f'(\lambda_j) \mid$. Bijovet difference and dispersive difference provide complementary information, and the strength of these differences can be predicted from the magnitude of tabulated anomalous scattering factors.

If f' and f'' have been evaluated, so that $a(\lambda)$, $b(\lambda)$ and $c(\lambda)$ are known, each of our measurements of $F_\lambda(\vec{h})$ at some wavelength gives us one instance of equation (7), and the separate instances may be treated as a system of simultaneous equations from which we want to obtain the quantities $|F_{0T}|$, $|F_{0A}|$ and $\Delta\varphi$. Actually we have two measurements for each wavelength, because the observation for F(-h,-k,-l) may be treated as an observation of F(h,k,l) with the value of f'' taken with opposite sign. So to obtain values of our three unknowns we will need at least three observations, which is to say data collected at two wavelengths with distinct scattering factors. Obviously it is better to be over-determined, so we would prefer data collected at three or more wavelengths. Now as written above, the equations are not linear. To solve them in practice (or at least as in the code implemented in the MADLSQ program (Hendrickson, 1985) we treat them instead as a set of linear equations in the four wavelength-independent factors in equation (7) imposing a Lagrangian constraint $(\sin^2\vartheta + \cos^2\vartheta = 1)$ in a non-linear least-squares procedure.

The treatment of data collected from crystals with more than one type of anomalous scattering atoms is exactly parallel, with the addition of two new quantities to be estimated, i.e. amplitude and phase for each new scattering type. So for two anomalous scattering types we have 5 unknowns and we will need data from a minimum of three wavelengths (F+ and F- at each of 3 wavelengths = 6 observations to derive 5 unknowns).

The set of derived $|F_{0A}|$ and $\Delta\varphi$ can be used to deduce the locations of anomalous scattering centers, in order to calculate the phase φ_{0A} of their contribution to the total scattering and the desired phase φ_{0T}. The simplest way to do this is through Patterson analysis; it amounts to solving an n atom structure, where n is the number of anomalous scattering atoms. There are many possible Patterson maps which can be calculated from the collected data. Of these the most familiar may be the Bijvoet Difference Patterson, calculated with coefficients $[F(+\vec{h}) - F(-\vec{h})]^2$. To increase the signal-to-noise ratio in the map one would logically choose the $F(+\vec{h})$ and $F(-\vec{h})$ values from the wavelengths λ with the largest expected value of f'' (fig. 5).

One problem with the estimates for $|F_{0A}|$ which come directly from the Karle/ Hendrickson equations is that the values are not always reasonable; e.g. sometimes the estimate for $|F_{0A}|$ is greater than the total scattering power of the atoms involved. Terwilliger (1994) suggests correcting this by using a Bayesian estimate for $|F_{0A}|$ predicated on the prior expected distribution of values: $P(F_{0A}) \propto \exp(-F_{0A}^2/\Sigma^2)$ where Σ^2 is the expected mean square value of $|F_{0A}|$ within a given resolution shell, given whatever we know about B values, scattering factors, etc. Furthermore we can also use prior

knowledge about the likely errors in our data to condition the probability of the observed quantities $\overline{F}$ = 1/2(|F+| + |F-|) and ΔF = (|F+| - |F-|)

$$P(\overline{F},\Delta F \mid F_{0A},F_{0T},\Delta\varphi) \propto \exp\left[-1/2\left(\frac{\varepsilon_{\overline{F}}^2}{E_{\overline{F}}^2+\sigma_{\overline{F}}^2}+\frac{\varepsilon_{\Delta F}^2}{E_{\Delta F}^2+\sigma_{\Delta F}^2}\right)\right] \tag{11}$$

where σ represents experimental uncertainty, E represents additional uncertainty and ε represents the difference between observed and calculated values of F and ΔF . After more of this sort of analysis we arrive at the Bayesian estimate for any quantity <x> that depends on $|F_{0T}|$, $|F_{0A}|$ and $\Delta\varphi$:

$$< x >= \frac{\int xP\left(F_{0A},F_{0T},\Delta\varphi \mid \left\{\overline{F},\Delta F\right\}_{\lambda_1\ldots\lambda_k}\right)dF_{0A}dF_{0T}d\Delta\varphi}{\int P\left(F_{0A},F_{0T},\Delta\varphi \mid \left\{\overline{F},\Delta F\right\}_{\lambda_1\ldots\lambda_k}\right)dF_{0A}dF_{0T}d\Delta\varphi} \tag{12}$$

The integration should properly run over all three variables $|F_{0T}|$, $|F_{0A}|$ and $\Delta\varphi$, but Terwilliger suggests taking $|F_{0T}|$ as being purely defined by its most probable value in order to save computational time.

4. Experimental Procedures

4.1 Feasibility of MAD experiments

The MAD technique cannot be applied to every crystal. In order for MAD phasing to be successful, the signal from the anomalous scatterers must be sufficiently large relative to the total scattering of the sample. The anomalous signal from each heavy atom depends on what that atom is, and the absorption edge of the scatterer must be inside the wavelength range of the beamline where the experiment will be performed. At the X-Ray Diffraction beamline of ELETTRA, with the standard Si (111) and Si (220) monochromator crystals, the range of possible wavelengths is 0.5 - 3 Å (4-25 keV). This allows, in principle, use of the K edges of elements 20 - 46 (including Fe, Cu, Se and Br) or the L-III edges of elements 50 and up (including Xe, Hg, Pt, U, lanthanides, etc.). Diffraction experiments have also been conducted at the S K edge (λ = 5.02 Å), but these require vacuum chambers

and very thin samples. Even experiments at the Ca K edge would be compromised by absorption.

The total signal depends on the number of ordered anomalous scatterers as well as on their nature. As an example, consider a 100 residue protein containing 2 Se atoms. The total number of electrons is approximately 5200. Of this, the two selenium atoms contribute 68. The single-wavelength anomalous signal depends on the imaginary component of the scattering factor f'', while the multiple-wavelength (dispersive) signal depends on the difference in scattering factors at the two wavelengths, $f'(1)-f'(2)$. These factors vary with the environment of the Se atoms, but typical values are at most 3.7 and 6.6 electrons, respectively, assuming suitable selection of wavelengths. The resulting ratio of anomalous signal to total structure factor may then be calculated according to the method of Hendrickson (1991), and is at most 4.0% for the Bijvoet and 3.5% for the dispersive case. Similar calculations can be applied to other typical scatterers, assuming 3% Bijvoet differences and 2% dispersive differences as reasonable signals.

4.2 Choice of correct wavelengths

As has been pointed out by Hendrickson (1985) it is advantageous to maximize both the Bijvoet differences within a data set and the dispersive differences between data sets. Thus it is best to choose the maximum of f'' at the so-called "white line", the minimum of f' at the inflection point, and one or more remote points at which f' is substantially closer to zero than at the edge.

The x-ray absorption spectrum of the anomalously scattering atoms in the crystal is measured by a simple x-ray detector mounted at right angles to the x-ray beam and in the horizontal plane to capture fluorescence as an indirect measure of absorption. This position reduces the x-ray scattering background and maximizes the signal-to-noise of the fluorescence. The fluorescence is related to f'', and over a small energy range can be considered roughly proportional to f''. From the absorption spectrum, monochromator positions are determined for the inflection point and the peak. The difference in f' between this inflection and a remote point should be as large as possible. Since the spectrum can vary rapidly around the minimum of f', even a small error in the position of the inflection point can result in much smaller dispersive differences than expected. The white line position is a maximum for f'' and gives rise to large Bijvoet differences within the data at that wavelength. The remote point is chosen on the high energy side and has a significant f'' although not as high as that at the white line. The exact location of this remote point depends on factors like the usable wavelength range of the particular instrument and the

convenience of wavelength changes. A fourth point is usually taken slightly below the edge, but as a rule it is generally preferable to have complete data at fewer wavelengths than partial data at more wavelengths.

The position and structure of absorption edges, as we mentioned before, are quite sensitive to the oxidation state and chemical environment of the absorbing atom. Therefore, scattering factors cannot be accurately determined from theoretical absorption spectra, and the absorption edges must be measured experimentally.

4.3 Data collection strategies

When using MAD data sets, where the signal is very often of the same magnitude of the standard deviation of the observations, it is necessary to take particular care to minimize error in differences between the structure factors measured at different wavelengths (dispersive differences) and between Friedel pairs (Bijvoet differences). The best approach is to minimize random errors by careful and repeated measurement, and to guarantee that each set of observations to be used for phasing has the same systematic error. This should be achieved by careful design of the experiment: first of all the same reflections should be measured from the same crystal, in the same orientation and, possibly, nearly at the same time. The development of techniques for the freezing of crystals and collection of data at 100 K has greatly eased the problem of MAD data collection. In this case, larger blocks of data can be collected at each wavelength to minimize the number of wavelength changes, thereby saving time and trouble.

After selection of the wavelengths for data collection, two different strategies can be chosen: in "mirror" geometry, the crystal is oriented with a mirror plane perpendicular to the spindle axis, and anomalous pairs appear on each image. In the "inverse beam" case data are collected over a small rotation range between φ_1 and φ_2 and the crystal is flipped 180 degrees in φ, followed by data collection between $180+\varphi_1$ and $180+\varphi_2$. In this geometry anomalous mates appear on pairs of images collected with spindle angles differing by 180 degrees. The dispersive differences are small compared to typical isomorphous differences for heavy atom derivatives, and the intensity changes can be as small as a few percent. Thus, for any given reflection, data for all the wavelengths are collected from the same crystal to allow the accurate measurement of dispersive differences. To ensure that Bijvoet differences are measured as accurately as possible, it is preferable to follow the mirror geometry method.

If it is not possible to orient the crystals in this way, then one has to use the inverse beam method, which ensures measurement of F(h,k,l) and F(-h,-k,-l) close together in

time. This strategy is used for each wavelength. An advantage of this method is that absorption corrections between Friedel mates are essentially non-existent. A major disadvantage is the additional amount of data collection; also, in methods where the phasing is done on individual sets of reflections rather than merging equivalent reflections first, bookkeeping of the data becomes more complicated.

Mirror geometry is clearly preferable in terms of reducing the number of exposures and insuring good scaling between anomalous pairs, and should generally be used when possible, especially when another data set is available for scaling purposes.

4.4 Analytical methods

Two approaches are conventionally used for phase determination based on anomalous diffraction measurement at multiple wavelengths. Probability methods adopted from MIR for single-wavelength anomalous scattering have been applied since the very beginning of MAD, even if some authors suggest that the lack of an actual native state makes this awkward. In the following we will describe the data analysis based on the Hendrickson approach as adapted from the formalism of Karle in the program MADLSQ. Another common software is MLPHARE, which exploits maximum-likelihood methods in phase calculation.

Diffraction data are reduced to integrated intensities with conventional programs like Mosflm or DENZO, then reflections at each wavelength are brought to a common scale applying a scale factor while keeping symmetry equivalent reflections separate. Since local scaling can help to remove systematic errors, data sets should not be merged before local scales are calculated and that the merging appropriate to the space group is carried out after phasing. The approach of merging symmetry equivalents is usually appropriate, but may not always be best, particularly in the case of large systematic errors, such as caused by absorption. What follows is the MAD analysis itself: a least squares fitting is made to extract from each phasing set the independent variables $|F_{0T}|$, $|F_{0A}|$ and $\Delta\varphi$ for the normal scattering contributions from all atoms (T) and from the anomalous centers alone (A). Only now symmetry equivalents are merged, as described before, to obtain a unique set of phased reflections. All the subsequent phase calculations require that the anomalous-scattering sites first be identified from Patterson or direct methods. As an example of the first method, in figure 6a we show a Harker section from such a Patterson map with coefficients $[F(+\bar{h}) - F(-\bar{h})]^2$ from a single Cu atom in the 96 residue metalloprotein CBP (Guss *et al.* 1989). The result is rather noisy because even at the optimal wavelength the maximal value of f'' is only 4.2e. The problem can be solved, instead of calculating any

map which uses only a subset of the data collected, using the newly estimated value for $| F_{0A} |$ to calculate a Patterson map with coefficients $| F_{0A} |^2$ (fig. 6b). Because all of the data contribute simultaneously to this map, it will be less noisy than a map calculated using only a subset of the data. The structure is then refined, but since the enantiomeric state of a structure is indeterminate from its normal diffraction data, the structure of the anomalous scattering centers contains an inherent ambiguity. This ambiguity is usually resolved by chemical reasonableness or by symmetry considerations.

References

Blundell, T.L., Johnson, L.N. (1976) in *Protein Crystallography* (Academic Press, London).

Drenth, J. (1994) in *Principles of Protein X-Ray Crystallography*. (Springer-Verlag, New York).

Glover, I.D., Denny, R.C., Nguti, N.D., McSweeney, S.M., Kinder, S.H., Thompson, A.W., Dodson, E.J., Wilkinson, A.J. and Tame, J.R.H. (1995) Acta Cryst. **D51**, 39.

Green, D.W., Ingram, V.M. and Perutz, M.F. (1954) Proc. R. Soc. **A255**, 287.

Guss, M., Merritt, E.A., Phizackerley, R.P., Hedman, B., Murata, M., Hodgson, K.O., and Freeman, H.C. (1989) Science **241**, 806.

Hendrickson, W.A. (1985) Trans. Am. Crystallogr. Assoc. **21**, 11.

Hendrickson, W.A., Smith, J.L., Phizackerley, R.P. and Merritt, E.A. (1988) Proteins **4**, 77.

Hendrickson, W.A. (1991) Science **254**, 51.

James, R.W. (1948) in *The Crystalline State* Vol II (Bell & Hyman, Ltd); republished as *The Optical Principles of the Diffraction of X-rays* (Ox Bow Press, Woodbridge, 1982).

Karle, J. (1980) Int. J. Quantum Chemistry **7**, 357.

Ramakrisnan V. and Biou, V. (1997) in *Methods in Enzymology*, Carter, C.W. Jr. and Sweet, R.M., Ed. (Academic Press, New York).

Templeton, L.K., Templeton, D.H., Phizackerley, R.P. and Hodgson, K.O. (1982) Acta Cryst. **A38**, 74.

Terwilliger, T.C. (1994) Acta Cryst. **D50**, 11 and Acta Cryst. **D50**, 17.

Tesmer, J.J.G., Stemmler, T.L., Penner-Hahn, J.E., Davisson, V.J. and Smith, J.L. (1994) Proteins **18**, 394.

Todd, A.R., Adams, A., Powell, H.R., Wilcock, D.J., Lausi, A., Zanini, F. and Cardin, C.J. (in press) Acta Cryst. D

Yang, W., Hendrickson, W.A., Crouch, R.J. and Satow, Y. (1990) Science **249**, 1398.

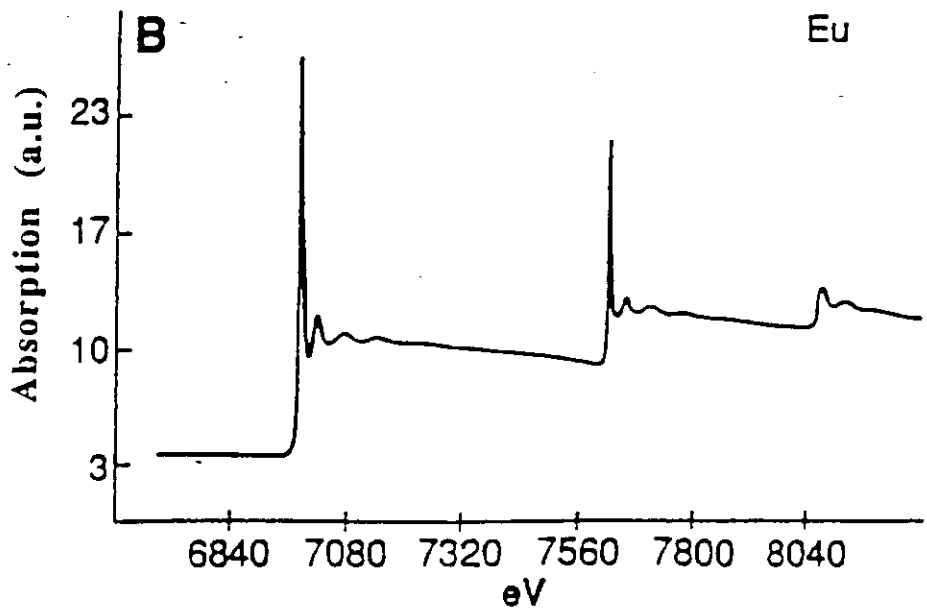

Fig. 1. Experimental values derived from an x-ray absorption spectrum of Eu-$(PhAcAc)_3$. The resonances from left to right are associated with the L_{III}, L_{II} and L_{I} transitions. The L_{III} maximum occurs at 6982.2 ev (1.7757 Å).

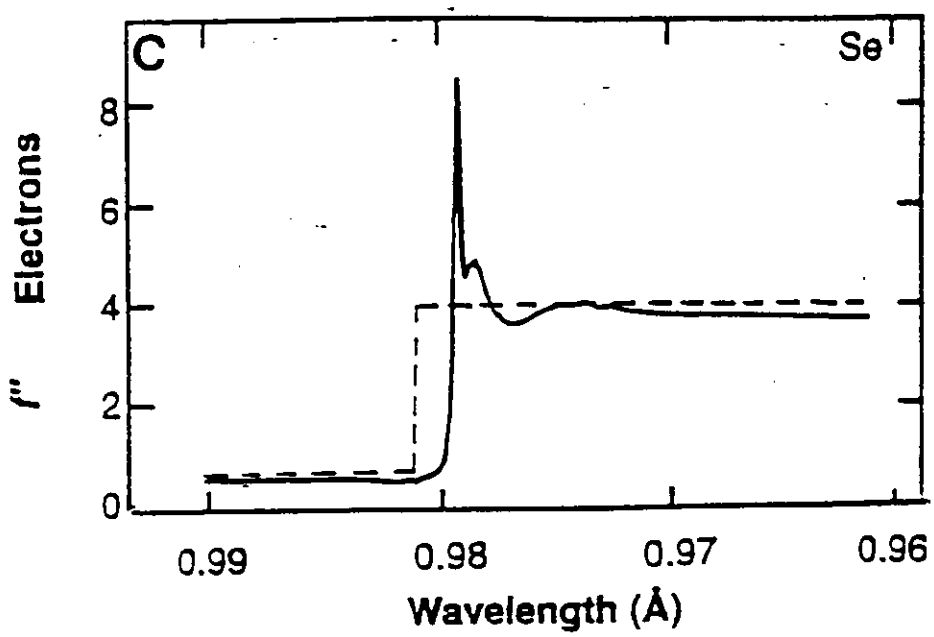

Fig. 2. Comparison of the Cromer-Liberman theoretical values of f'' (dotted line) with the experimental values (continuous line) for the selenium site of selenomethionyl thioredoxin.

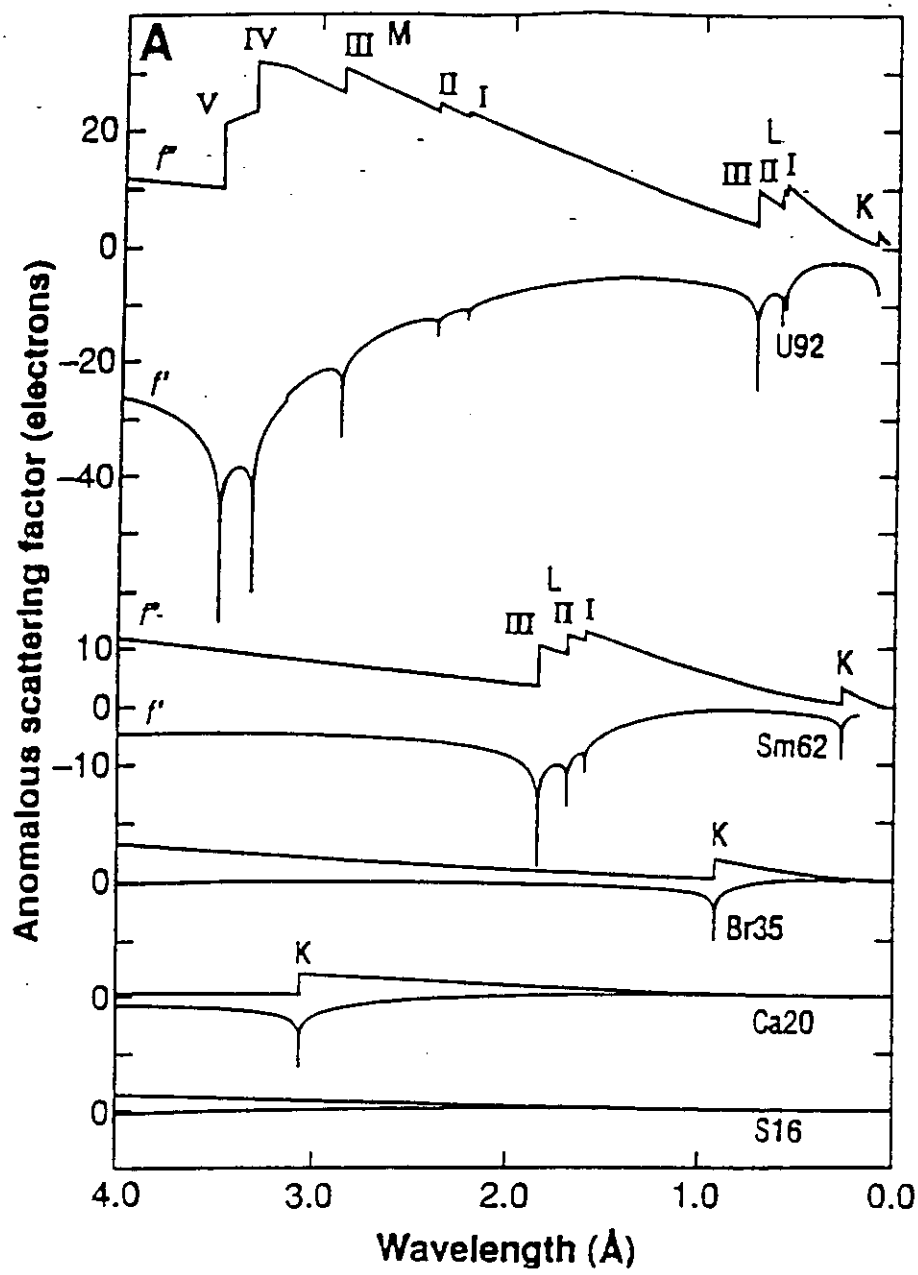

Fig. 3. Anomalous spectra for selected isolated elements. For each element the imaginary component f'' is drawn in the upper curve and the real component f' is in the lower curve.

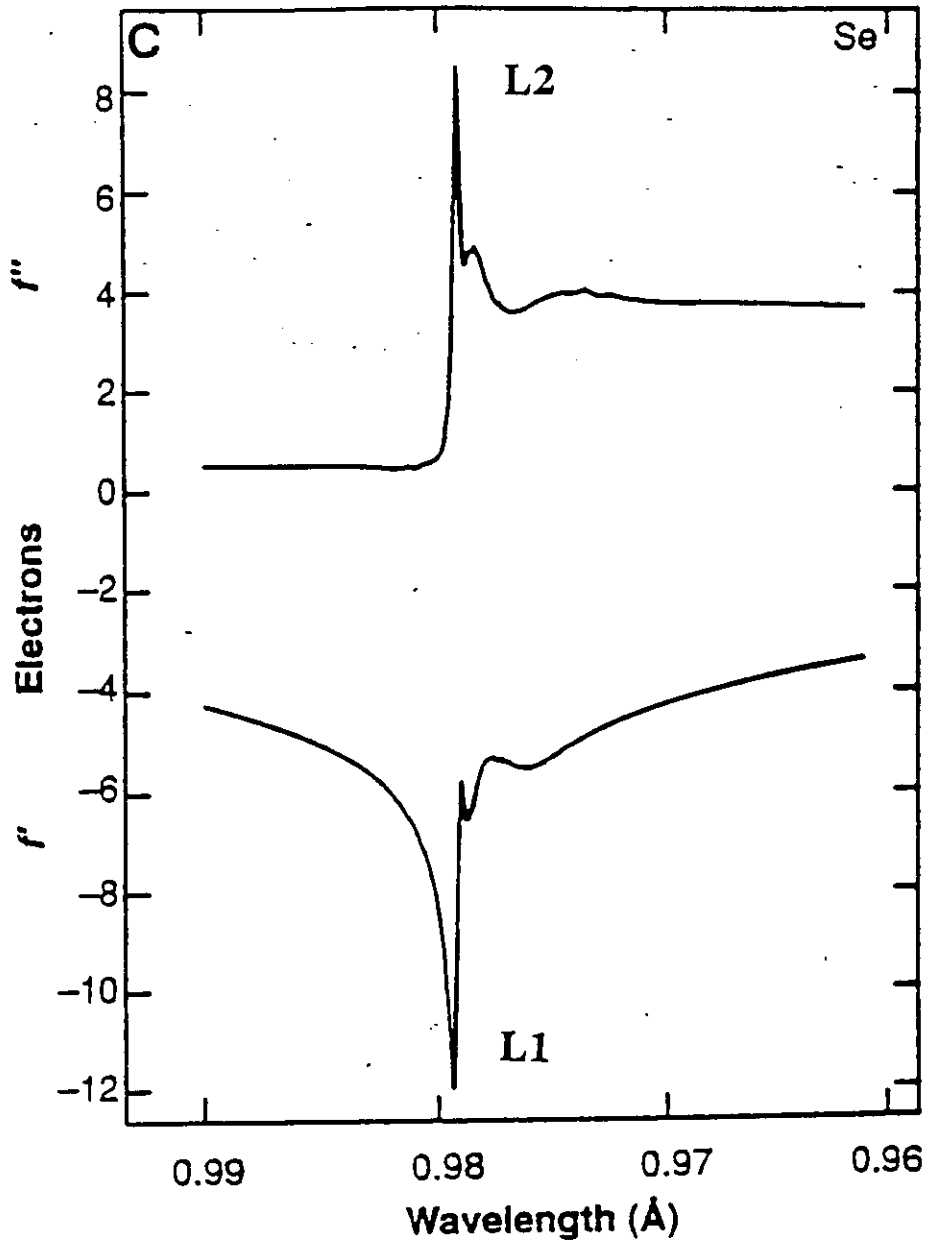

Fig. 4. The variation of the real (f') and imaginary (f'') components of the anomalous scattering around the K-edge of selenium from an experimental X-ray absorption spectrum of selenomethionyl thioredoxin from *E. Coli* (Hendrickson, 1988). The three wavelengths chosen for diffraction measurements in a MAD experiments are designated as follows: L1 is the minimum of f', called the "inflection point" or "edge"; L2 is the maximum of f'', called the "white line"; and L3 is a remote point at 0.93 Å which lies well on the high wavelength side of the interval shown in the graph.

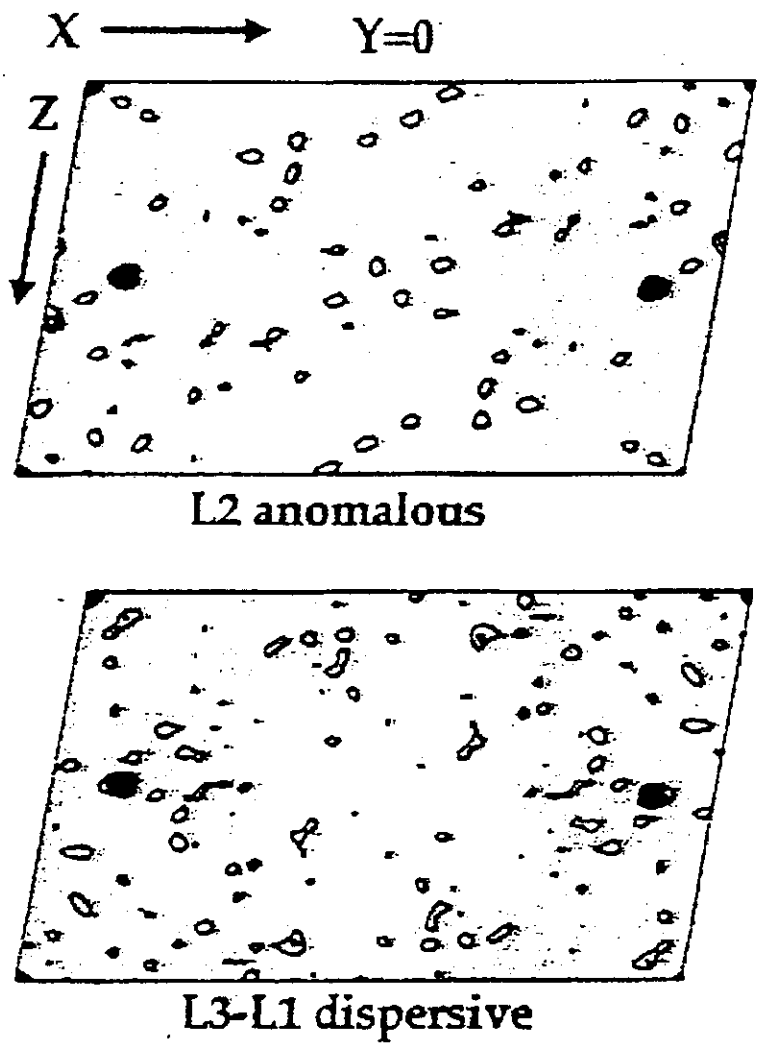

Fig. 5. Harker sections of Patterson maps from MAD data on IF3-C, the C-terminal domain of translational initiation factor 3, which crystallizes in the space group C2. The top section is from the anomalous-Patterson map calculated from the L2 white line data. The bottom section is from a difference-Patterson map obtained by treating L1 (the inflection point) as native and L3 (the remote point) as derivative.

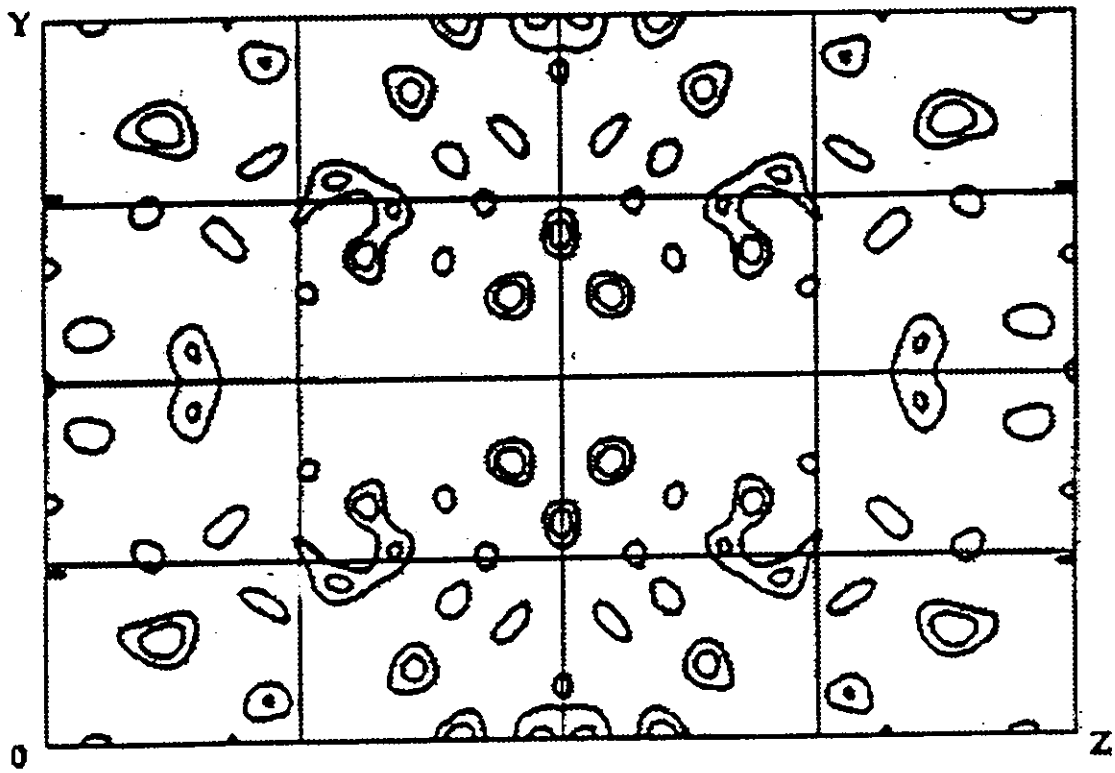

Fig. 6a. Harker section of a Bijvoet difference Patterson map from a single Cu atom in the 96 residue metalloprotein CBP. The data were taken at 1.3771Å with a f'' of 4.17e.

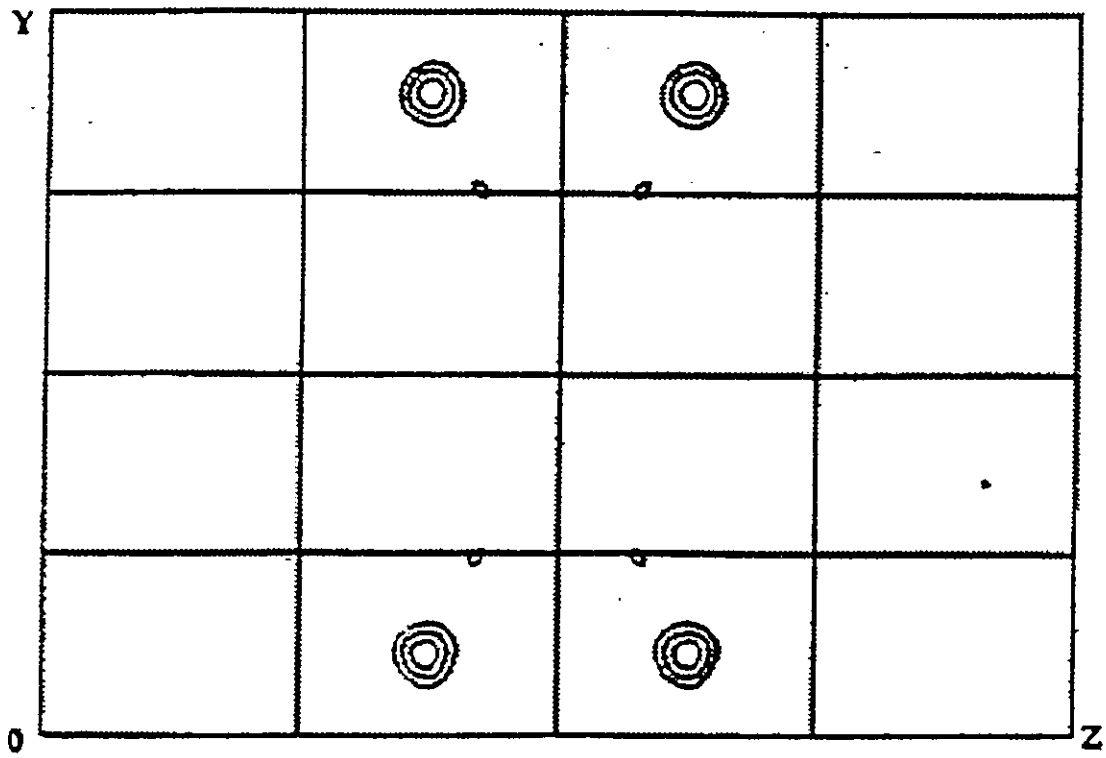

Fig. 6b. Harker section of a $|F_{0A}|^2$ Patterson map from the same sample of fig. 5a and data taken at four wavelengths.